J|A|C|S
ARTICLES
Published on Web 06/13/2006

Structure and Enhanced Reactivity Rates of the D_{5h} $Sc_3N@C_{80}$ and $Lu_3N@C_{80}$ Metallofullerene Isomers: The Importance of the Pyracylene Motif

Ting Cai,[†] Liaosa Xu,[†] Mark R. Anderson,[†] Zhongxin Ge,[†] Tianming Zuo,[†] Xuelei Wang,[†] Marilyn M. Olmstead,[‡] Alan L. Balch,*[,‡] Harry W. Gibson,*[,†] and Harry C. Dorn*[,†]

Contribution from the Departments of Chemistry, Virginia Polytechnic Institute and State University, Blacksburg, Virginia 24060-0212, and University of California, Davis, California 95616

Received March 6, 2006; E-mail: albalch@ucdavis.edu; hwgibson@vt.edu; hdorn@vt.edu

Abstract: In this paper we report enhanced reactivity of the D_{5h} isomers in comparison with the more common I_h isomers of $Sc_3N@C_{80}$ and $Lu_3N@C_{80}$ toward Diels−Alder and 1,3-dipolar tritylazomethine ylide cycloaddition reactions. Also, the structure of the D_{5h} isomer of $Sc_3N@C_{80}$ has been determined through single-crystal X-ray diffraction on D_{5h}-$Sc_3N@C_{80}$·Ni(OEP)·2benzene (OEP = octaethylporphyrin). The Sc_3N portion of D_{5h}-$Sc_3N@C_{80}$ is strictly planar, but the plane of these four atoms is tipped out of the noncrystallographic, horizontal mirror plane of the fullerene by 30°. The combination of short bond length and high degree of pyramidization for the central carbon atoms of the pyracylene sites situated along a belt that is perpendicular to the C_5 axis suggests that these are the sites of greatest reactivity in the D_{5h} isomer of $Sc_3N@C_{80}$. Consistent with the observation of higher reactivity observed for the D_{5h} isomers, cyclic voltammetry and molecular orbital (MO) calculations demonstrate that the D_{5h} isomers have slightly smaller energy gaps than those of the I_h isomers. The first mono- and bis-adducts of D_{5h} $Sc_3N@C_{80}$ have been synthesized via 1,3-dipolar cycloaddition of tritylazomethine ylide. The NMR spectrum for the monoadduct **2b** is consistent with reaction at the 6,6-ring juncture in the pyracylene unit of the D_{5h} $Sc_3N@C_{80}$ cage and is the thermodynamically stable isomer. On the other hand, monoadduct **2a** undergoes thermal conversion to other isomeric monoadducts, and three possible structures are proposed.

Introduction

Endohedral metallofullerenes (EMF) have attracted increasing attention during past decades for their potential applications in the fields of biomedicine and nanomaterial sciences.[1] The chemical and electronic properties and exohedral chemical functionalizations for various mono- and di-metallofullerenes have been extensively studied.[2] In 1999, a novel stable four-atom molecular cluster endohedral fullerene, icosahedrally (I_h) symmetrical $Sc_3N@C_{80}$, was prepared in remarkably high yield by the use of the trimetallic nitride template (TNT) process.[3] Computational and experimental results demonstrate that the C_{80} cage is stabilized by the transfer of six electrons from the internal trimetallic nitride cluster, resulting in a closed shell electronic structure, i.e., $(Sc_3N)^{6+}C_{80}^{6-}$.[4] Long-time molecular dynamics simulations followed by quantitative DFT-NMR calculations of the ^{13}C NMR chemical shifts of the $Sc_3N@C_{80}$

[†] Virginia Polytechnic Institute and State University.
[‡] University of California, Davis.

(1) *Endofullerenes: A New Family of Carbon Clusters*; Akasaka, T., Nagase, S., Eds.; Kluwer: Dordrecht, The Netherlands, 2002. (b) Shinohara, H. *Rep. Prog. Phys.* **2000**, *63*, 843−892. (c) Nagase, S.; Kobayashi, K.; Akasaka, T.; Wakahara, T. In *Fullerenes: Chemistry, Physics and Technology*; Kadish, K., Ruoff, R. S., Eds.; John Wiley & Sons: New York, 2000; pp 395−436. (d) Wilson, L. J.; Cagle, D. W.; Thrash, T. P.; Kennel, S. J.; Mirzadeh, S.; Alford, J. M.; Ehrhardt, G. J. *Coord. Chem. Rev.* **1999**, *190*−*192*, 199−207. (e) Cagle, D. W.; Kennel, S. J.; Mirzadeh, S.; Alford, J. M.; Wilson, L. J. *Proc. Natl. Acad. Sci. U.S.A.* **1999**, *96*, 5182−5187. (f) Kato, H.; Kanazawa, Y.; Okumura, M.; Taninaka, A.; Yokawa, T.; Shinohara, H. *J. Am. Chem. Soc.* **2003**, *125*, 4391−4397. (g) Kobayashi, S.; Mori, S.; Iida, S.; Ando, H.; Takenobu, T.; Taguchi, Y.; Fujiwara, A.; Taninaka, A.; Shinohara, H.; Iwasa, Y. *J. Am. Chem. Soc.* **2003**, *125*, 8116−8117.

(2) (a) Suzuki, T.; Kikuchi, K.; Oguri, F.; Nakao, Y.; Suzuki, S.; Achiba, Y.; Yamamoto, K.; Funasaka, H.; Takahashi, T. *Tetrahedron* **1996**, *52*, 4973−4982. (b) Maeda, Y.; Miyashita, J.; Hasegawa, T.; Wakahara, T.; Tsuchiya, T.; Feng, L.; Lian, Y.; Akasaka, T.; Kobayashi, K.; Nagase, S.; Kako, M.; Yamamoto, K.; Kadish, K. M. *J. Am. Chem. Soc.* **2005**, *127*, 2143−2146. (c) Akasaka, T.; Kato, T.; Kobayashi, K.; Nagase, S.; Yamamoto, K.; Funasaka, H.; Takahashi, T. *Nature* **1995**, *374*, 600−601. (d) Akasaka, T.; Nagase, S.; Kobayashi, K.; Suzuki, T.; Kato, T.; Yamamoto, K.; Funasaka, H.; Takahashi, T. *J. Chem. Soc., Chem. Commun.* **1995**, 1343−1344. (e) Akasaka, T.; Okubo, S.; Kondo, M.; Maeda, Y.; Wakahara, T.; Kato, T.; Suzuki, T.; Yamamoto, K.; Kobayashi, K.; Nagase, S. *Chem. Phys. Lett.* **2000**, *319*, 153−156. (f) Yamada, M.; Feng, L.; Wakahara, T.; Maeda, Y.; Lian, Y.; Kako, M.; Akasaka, T.; Kato, T.; Kobayashi, K.; Nagase, S. *J. Phys. Chem. B* **2005**, *109*, 6049−6051. (g) Maeda, Y.; Miyashita, J.; Hasegawa, T.; Wakahara, T.; Tsuchiya, T.; Nakahodo, T.; Akasaka, T.; Mizorogi, N.; Kobayashi, K.; Nagase, S.; Kato, T.; Ban, N.; Nakajima, H.; Watanabe, Y. *J. Am. Chem. Soc.* **2005**, *127*, 12190−12191. (h) Yamada, M.; Nakahodo, T.; Wakahara, T.; Tsuchiya, T.; Maeda, Y.; Akasaka, T.; Kako, M.; Yoza, K.; Horn, E.; Mizorogi, N.; Kobayashi, K.; Nagase, S. *J. Am. Chem. Soc.* **2005**, *127*, 14570−14571.

(3) Stevenson, S.; Rice, G.; Glass, T.; Harich, K.; Cromer, F.; Jordan, M. R.; Craft, J.; Hadju, E.; Bible, R.; Olmstead, M. M.; Maltra, K.; Fisher, A. J.; Balch, A. L.; Dorn, H. C. *Nature* **1999**, *401*, 55−57.

(4) (a) Kobayashi, K.; Sano, Y.; Nagase, S. *J. Comput. Chem.* **2001**, *22*, 1353−1358. (b) Campanera, J. M.; Bo, C.; Olmstead, M. M.; Balch, A. L.; Poblet, J. M. *J. Phys. Chem. A* **2002**, *106*, 12356−12364. (c) Olmstead, M. M.; de Bettencourt-Dias, A.; Duchamp, J. C.; Stevenson, S.; Marciu, D.; Dorn, H. C.; Balch, A. L. *Angew. Chem., Int. Ed.* **2001**, *40*, 1223−1225. (d) Krause, M.; Kuzmany, H.; Georgi, P.; Dunsch, L.; Vietze, K.; Seifert, G. *J. Chem. Phys.* **2001**, *115*, 6596−6605. (e) Alvarez, L.; Pichler, T.; Georgi, P.; Schwieger, T.; Peisert, H.; Dunsch, L.; Hu, Z.; Knupfer, M.; Fink, J.; Bressler, P. Mast, M.; Golden, M. S. *Phys. Rev. B* **2002**, *66*, 035107/1-035107/7.

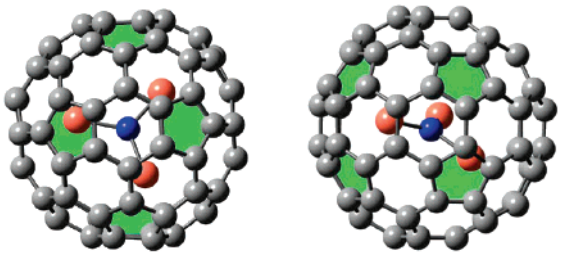

Figure 1. (Left) $Sc_3N@C_{80}$ I_h isomer. (Right) $Sc_3N@C_{80}$ D_{5h} isomer.

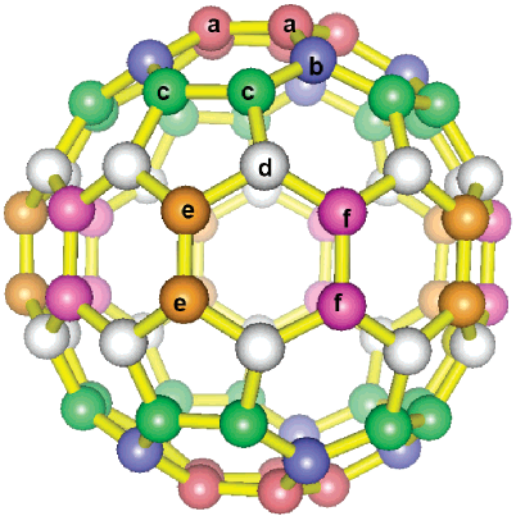

Figure 2. A schematic diagram of the carbon cage of the D_{5h} C_{80} isomer showing the six bands of different types of carbon atoms.

I_h isomer reproduced the two-line experimental spectrum.[5] Two other Sc_3N EMF family members, the D_{3h} symmetrical $Sc_3N@C_{78}$[6] and the D_3 symmetrical non-IPR (isolated-pentagon rule) $Sc_3N@C_{68}$[7] were also discovered. Thus far the family of TNT-EMFs has been expanded to other metals $A_3N@C_{2n}$ (A = Y, Gd, Tb, Dy, Ho, Er, Tm, and Lu; $38 \leq n \leq 49$).[4d,8]

In an earlier study,[9] we proposed that a relatively small amount of the D_{5h} isomer of $Sc_3N@C_{80}$ existed in samples dominated by the I_h isomer based on high performance liquid chromatography (HPLC) and ^{13}C NMR. The structures of these two isomers are compared in Figure 1. Figure 2 shows a schematic diagram of the D_{5h} isomer of the C_{80} cage with its six different types of carbon atoms arranged into six colored layers.

Dunsch and co-workers used HPLC to separate I_h and D_{5h} isomers for various trimetallic nitride endohedral metallofullerenes, including $Sc_3N@C_{80}$,[10] $Tm_3N@C_{80}$,[8e] and $Dy_3N@C_{80}$.[8c] Since the retention times of the two isomers are similar, to achieve better separation, a linear combination of two HPLC columns and multiple injections were applied to afford pure isomers. Compared with the I_h isomer, a relatively smaller optical energy gap, i.e., a longer onset wavelength λ_{max} value, was reported for the D_{5h} isomers by visible−NIR spectroscopy.[8c,e,10] On the basis of different oxidation potentials for $Sc_3N@C_{80}$ I_h and D_{5h} isomers, Echegoyen and co-workers reported an electrochemical method to oxidize the D_{5h} isomer selectively.[11] The unoxidized I_h isomer could then be purified by removing the radical cation of the D_{5h} isomer from the silica column. Based on density functional theoretical (DFT) methods and Gibbs energy calculations, Slanina and Nagase recently calculated the observed populations of 10% and 17% for the D_{5h} $Sc_3N@C_{80}$ isomer at temperatures of 2100 and 2340 K, respectively.[12] Very recently, Yang and Dunsch reported the third stable trimetallic nitride encapsulated C_{80} cage; the $Dy_3N@C_{80}$ isomer with a proposed D_{5d} symmetrical structure was isolated and characterized by optical and vibrational spectroscopy.[13]

In this paper, we explore the Diels−Alder cycloaddition reactions of $A_3N@C_{80}$ (A = Sc, Lu) with cyclopentadiene-functionalized resin as a method for purification of mixtures of I_h and D_{5h} TNT-EMFs. Both D_{5h} $Sc_3N@C_{80}$ and $Lu_3N@C_{80}$ exhibit higher reactivity than those of the respective I_h isomers. Cyclic voltammetry and theoretical molecular orbital (MO) calculations have also been carried out for $Sc_3N@C_{80}$ and $Lu_3N@C_{80}$ in order to understand the relative stabilities and reactivities of the D_{5h} and I_h isomers. Although several exohedral derivatives of TNT-EMF I_h isomers have been synthesized and characterized,[14,15] no derivatives of the D_{5h} isomers have been previously reported. Herein, for the first time we report the synthesis and characterization of *N*-tritylpyrrolidino mono- and bis-adducts of the D_{5h} isomer of $Sc_3N@C_{80}$ through the Prato reaction.[16] The possible cycloaddition reaction sites for the two monoadducts of the D_{5h} isomer are discussed based on ^1H NMR evidence and other data deduced from DFT calculations, electrochemistry, and X-ray crystallography.

Results and Discussion

I. Crystallographic Determination of the Structure of the D_{5h} Isomer of $Sc_3N@C_{80}$. Since we have repeatedly demonstrated that cocrystallization with metallo-octaethylporphyrins, M^{II}(OEP) (M = Ni, Co), produces samples with sufficient order

(5) Heine, T.; Vietze, K.; Seifert, G. *Magn. Reson. Chem.* **2004**, *42*, S199−S201.
(6) Olmstead, M. M.; Bettencourt-Dias, A.; Duchamp, J. C.; Stevenson, S.; Marciu, D.; Dorn, H. C.; Balch, A. L. *Angew. Chem., Int. Ed.* **2001**, *40*, 1223−1225.
(7) (a) Stevenson, S.; Fowler, P. W.; Heine, T.; Duchamp, J. C.; Rice, G.; Glass, T.; Harich, K.; Hajdu, E.; Bible, R.; Dorn, H. C. *Nature* **2000**, *408*, 427−428. (b) Olmstead, M. M.; Lee, H. M.; Duchamp, J. C.; Stevenson, S.; Marciu, D.; Dorn, H. C.; Balch, A. L. *Angew. Chem., Int. Ed.* **2003**, *42*, 900−903.
(8) (a) Krause, M.; Dunsch, L. *Angew. Chem., Int. Ed.* **2005**, *44*, 1557−1560. (b) Feng, L.; Xu, J. X.; Shi, Z. J.; He, X. R.; Gu, Z. N. *Gaodeng Xuexiao Huaxue Xuebao* **2002**, *23*, 996−998. (c) Yang, S.; Dunsch, L. *J. Phys. Chem. B* **2005**, *109*, 12320−12328. (d) Dunsch, L.; Georgi, P.; Krause, M.; Wang, C. R. *Synth. Met.* **2003**, *135*−*136*, 761−762. (e) Krause, M.; Wong, J.; Dunsch, L. *Chem.*−*Eur. J.* **2005**, *11*, 706−711. (f) Iezzi, E. B.; Duchamp, J. C.; Fletcher, K. R.; Glass, T. E.; Dorn, H. C. *Nano Lett.* **2002**, *2*, 1187−1190. (g) Stevenson, S.; Lee, H. M.; Olmstead, M. M.; Kozikowski, C.; Stevenson, P.; Balch, A. L. *Chem. Eur. J.* **2002**, *8*, 4528−4535. (h) Stevenson, S.; Phillips, J. P.; Reid, J. E.; Olmstead, M. M.; Rath, S. P.; Balch, A. L. *Chem. Commun.* **2004**, 2814−2815.
(9) Duchamp, J. C.; Demortier, A.; Fletcher, K. R.; Dorn, D.; Iezzi, E. B.; Glass. T.; Dorn, H. C. *Chem. Phys. Lett.* **2003**, *375*, 655−659.
(10) Krause, M.; Dunsch, L. *ChemPhysChem* **2004**, *5*, 1445−1450.
(11) Elliott, B.; Yu, L.; Echegoyen, L. *J. Am. Chem. Soc.* **2005**, *127*, 10885−10888.
(12) Slanina, Z.; Nagase, S. *ChemPhysChem* **2005**, *6*, 2060−2063.
(13) Yang, S.; Dunsch, L. *Chem.*−*Eur. J.* **2006**, *12*, 413−419.
(14) (a) Iezzi, E. B.; Duchamp, J. C.; Harich, K.; Glass, T. E.; Lee, H. M.; Olmstead, M. M.; Balch, A. L.; Dorn, H. C. *J. Am. Chem. Soc.* **2002**, *124*, 524−525. (b) Lee, H. M.; Olmstead, M. M.; Iezzi, E.; Duchamp, J. C.; Dorn, H. C.; Balch, A. L. *J. Am. Chem. Soc.* **2002**, *124*, 3494−3495. (c) Stevenson, S.; Stephen, R. R.; Amos, T. M.; Cadorette, V. R.; Reid, J. E.; Phillips, J. P. *J. Am. Chem. Soc.* **2005**, *127*, 12776−12777.
(15) (a) Cardona, C. M.; Kitaygorodskiy, A.; Ortiz, A.; Herranz, M. A.; Echegoyen, L. *J. Org. Chem.* **2005**, *70*, 5092−5097. (b) Cardona, C. M.; Kitaygorodskiy, A.; Echegoyen, L. *J. Am. Chem. Soc.* **2005**, *127*, 10448−10453. (c) Cai, T.; Ge, Z.; Iezzi, E. B.; Glass, T. E.; Harich, K.; Gibson, H. W.; Dorn, H. C. *Chem. Commun.* **2005**, 3594−3596.
(16) (a) Prato, M.; Maggini, M. *Acc. Chem. Res.* **1998**, *31*, 519−526. (b) Maggini, M.; Scorrano, G.; Prato, M. *J. Am. Chem. Soc.* **1993**, *115*, 9798−9799.

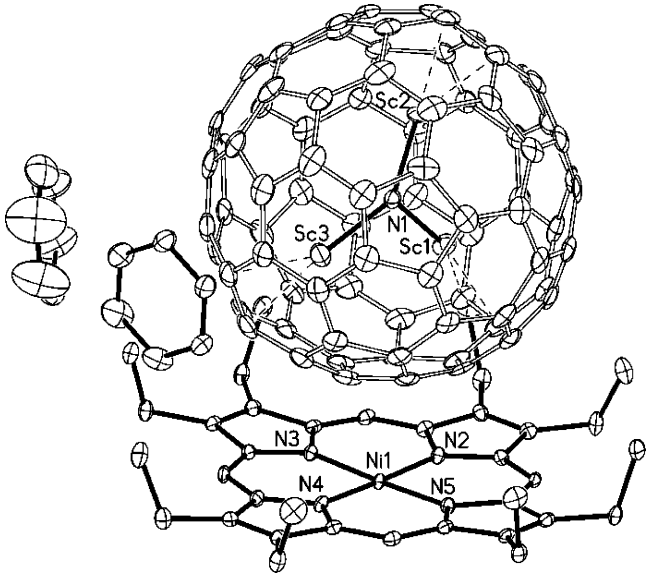

Figure 3. A view of the contents of the asymmetric unit in the D_{5h} isomer of $Sc_3N@C_{80}$·Ni(OEP)·2benzene with 50% thermal ellipsoids.

to allow structure determination,[3,4c,6,7b,17] benzene solutions of the D_{5h} isomer of $Sc_3N@C_{80}$ and Ni^{II}(OEP) were allowed to slowly diffuse together. Black papallelepipeds of the product were obtained and utilized in the crystal structure determination.

Figure 3 shows a drawing of the four molecules present in the asymmetric unit of the compound. None of these has any crystallographically imposed symmetry. As usual, all eight ethyl groups of the porphyrin surround the fullerene. The closest contact between the porphyrin and the endohedral is the 2.812(3) Å separation between Ni and C46. Remarkably, both the carbon cage and its contents are fully ordered.

Figure 4 shows two drawings of the fullerene itself. Part A shows a view down the noncrystallographic, five-fold axis of the cage, while part B shows a view perpendicular to that five-fold axis. As these drawings show, the Sc_3N portion is strictly planar (the sum of the three Sc−N−Sc angles is 359.94°), but the plane of these four atoms is tipped out of the noncrystallographic horizontal mirror plane of the fullerene by 30°. The geometry of the Sc_3N portion is rather irregular with a variety of Sc−N distances (Sc1−N, 2.014(2), Sc2−N, 2.031(2); Sc3−N, 2.041(2) Å) and N−Sc−N angles (Sc1−N−Sc2, 121.12(11); Sc1−N−Sc3, 107.21(10); Sc2−N−Sc3, 131.61(11)°). Each scandium ion is in close proximity to a pair of carbon atoms of the fullerene. Sc1 is located over a c−d bond involving C64 and C44, Sc2 sits over an e−e bond involving C24 and C57, and Sc3 is situated near a d−e bond involving C31 and C32.

The C−C bond distances in the carbon cage of D_{5h} $Sc_3N@C_{80}$ show greater variation than was observed in the corresponding I_h isomer. In I_h $Sc_3N@C_{80}$ there are only two types of C−C bonds. Those at the junction of two hexagons have an average distance of 1.421(18) Å, while those at the junction of a pentagon and a hexagon have an average distance of 1.437(15) Å.[14b] In the D_{5h} isomer of $Sc_3N@C_{80}$, the f−f bonds are the longest C−C bonds, while the e−e bonds are the shortest. These bonds alternate about the horizontal plane of the cage and lie in a direction parallel to the 5-fold axis. The short e−e C−C bonds (average distance, 1.396 Å) are in pyracylene sites where two hexagons abut with pentagons at either end, while the long f−f bonds (average distance 1.462 Å) are in pyrene sites. This is the first crystallographically characterized fullerene cage to have such pyrene sites. The other C−C bond lengths have the following average values (Å): a−a, 1.434; a−b, 1.420; b−c, 1.419; c−c, 1.438; c−d, 1.451; d−e, 1.434; d−f, 1.432. In all cases the C−C bonds nearest the three scandium ions have been omitted in calculating these average distances. The proximities of these pairs of carbon atoms closest to the scandium atoms appear to lengthen the C−C bonds between them.

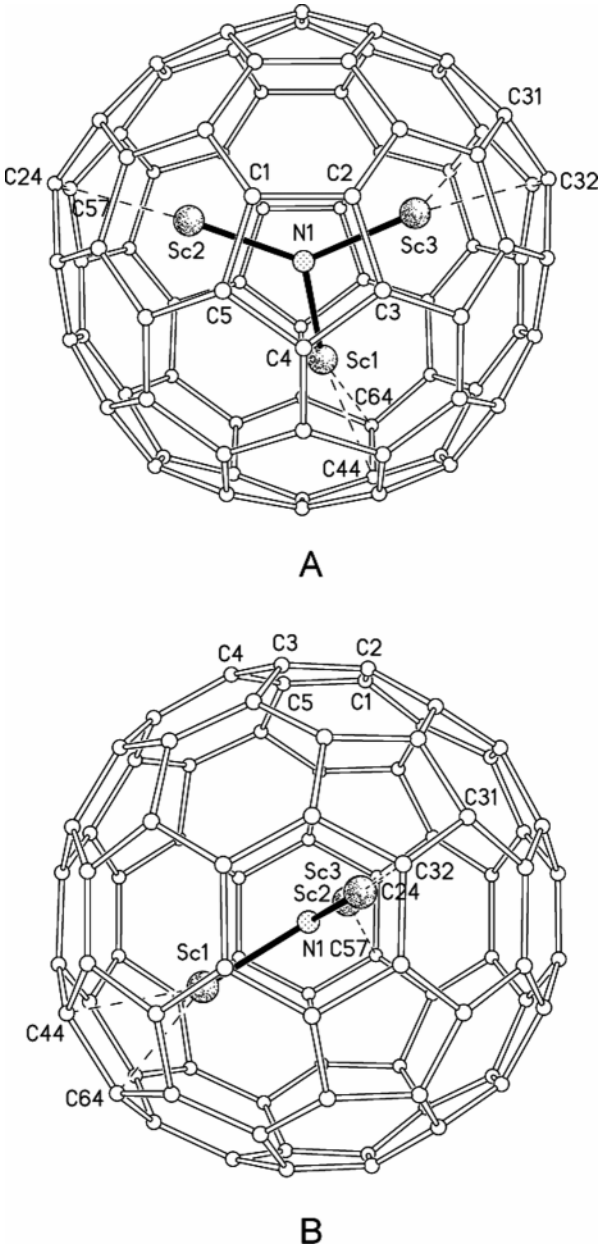

Figure 4. Two views of the endohedral fullerene in the D_{5h} isomer of $Sc_3N@C_{80}$·Ni(OEP)·2benzene. (Upper) Looking down the fullerene five-fold axis. (Lower) Looking perpendicular to the fullerene five-fold axis which is vertical in this view. For clarity, all atom positions are shown as circles of uniform size depending upon atom type.

The pyramidization angles, θ_p,[18] (θ_p for graphite = 0°; θ_p for C_{60} = 11.6°) for the individual fullerene carbons of D_{5h} $Sc_3N@C_{80}$ also show some interesting variations. The average pyramidization angles for the different types of carbon atoms

(17) Lee, H. M.; Olmstead, M. M.; Suetsuna, T.; Shimotani, H.; Dragoe, N.; Cross, R. J.; Kitazawa, K.; Balch, A. L. *Chem. Commun.* **2002**, 1352−1353.

are: a, 10.6°; b, 8.9°; c, 10.1°; d, 10.2°; e, 10.5°; and f, 8.4°. In averaging these values, those carbon atoms nearest the scandium ions have been omitted since the carbon atoms near scandium have particularly high pyramidization as follows: C64, 13.0°; C44, 12.9°; C24, 13.9°; C57, 11.3°; C31, 12.5°; C32, 13.8°. Similarly high pyramidization angles were seen for those carbon atoms nearest the scandium ions in a functionalized version of the I_h isomer of $Sc_3N@C_{80}$.[14b] The carbon atom nearest the porphyrin, C46, exhibits an unusually low θ_p of 8.7° for a carbon atom of the d-type. Likewise C47 which is the next nearest carbon to the porphyrin has a low θ_p of 7.6°, the lowest θ_p value seen for any of the f-type carbon atoms. For the other carbon atoms, the highest pyramidization is seen for the a-type carbon atoms at the poles of the carbon cage and for the e-type carbon atoms that surround the middle of the molecule. Notice that there is a pronounced alternation about the middle of the fullerene with the e-type carbon atoms showing a high degree of pyramidization and the f-type carbon atoms displaying the lowest degree of pyramidization seen anywhere in the molecule.

The combination of short bond length and high degree of pyramidization for the central carbon atoms of the pyracylene sites at the center of the carbon cage suggest that these may be the sites of greatest reactivity in the D_{5h} isomer of $Sc_3N@C_{80}$. The two carbons atoms at the center of pyracylene sites are generally the positions of highest chemical reactivity on empty cage fullerenes, but the I_h isomer of $Sc_3N@C_{80}$ lacks such sites. The lack of this structural feature offers some insight into the low degree of chemical reactivity of the I_h isomer of $Sc_3N@C_{80}$. In contrast the D_{5h} isomer of $Sc_3N@C_{80}$ is more reactive, and the NMR data for the mono-(*N*-tritylpyrrolidino) derivative of the D_{5h} isomer described below is consistent with the crystallographic work suggesting that the e−e bonds at the middle of this metallofullerene are the initial sites of addition.

II. Reactivity Comparisons. a. Kinetic Stability. Recently, using the cyclopentadiene-functionalized resin **1**, macroscopic quantities of high purity TNT-EMF were directly and expeditiously obtained from crude soots or extracts[19] by taking advantage of significantly different kinetic stabilities between TNT-EMFs and other fullerenes (empty cage fullerenes and classical endohedral metallofullerenes).[20,21] To explore the reactivity differences between I_h and D_{5h} isomers of TNT-EMFs, mixtures of $A_3N@C_{80}$ (A = Sc or Lu) I_h and D_{5h} were treated with large excesses of the cyclopentadiene-functionalized resin **1** (finely ground) under vigorous stirring at room temperature. The Diels−Alder cycloaddition reactions of TNT-EMFs with resin **1** were assumed to be under pseudo-first-order conditions. The concentration of $A_3N@C_{80}$ was monitored by HPLC.

Aihara's minimum bond resonance energy (min BRE) calculations[20a] and the calculated HOMO−LUMO energy gaps for the C_{80}^{6-} isomers[20a,22] suggested that the D_{5h} C_{80} cage with six negative charges is slightly more reactive than the I_h analogue. Figure 5 illustrates the different reactivities between TNT-EMF I_h and D_{5h} isomers with cyclopentadiene-functionalized resin **1** (Scheme 1). In Figure 5a, the D_{5h} $Sc_3N@C_{80}$ eluted later than the I_h isomer and appeared as a shoulder on the I_h chromatographic peak. The ratio of I_h to D_{5h} isomer peaks increased with reaction time, indicating that the D_{5h} isomer reacted faster than the I_h isomer in this competitive reaction. The D_{5h} $Sc_3N@C_{80}$ was almost completely removed from the original mixture after two weeks. A similar reactivity pattern was also observed for I_h and D_{5h} isomers of $Lu_3N@C_{80}$ (Figure 5b). The isomers of $Lu_3N@C_{80}$ were better resolved than those of $Sc_3N@C_{80}$ under the same HPLC conditions. The short elution time peak was the I_h $Lu_3N@C_{80}$,[8f] and the later one was the D_{5h} isomer. These assignments were confirmed by both mass spectrometry and ^{13}C NMR spectroscopy.

In the ^{13}C NMR spectrum of the $Lu_3N@C_{80}$ D_{5h} isomer (see Supporting Information), the chemical shifts for the six peaks (135.5, 138.1, 138.2, 143.2, 144.7, and 149.0 ppm), representing the six different types of carbon atoms on the D_{5h} C_{80} cage, and their relative intensities are very consistent with the reported assignment for the ^{13}C NMR spectrum of the $Sc_3N@C_{80}$ D_{5h} isomer.[9] After normalizing the I_h chromatographic peaks to the same height, the peaks for the D_{5h} $Lu_3N@C_{80}$ were found to decrease with increasing reaction time, again indicating the higher reactivity of the D_{5h} isomer. As a result of the distinctly

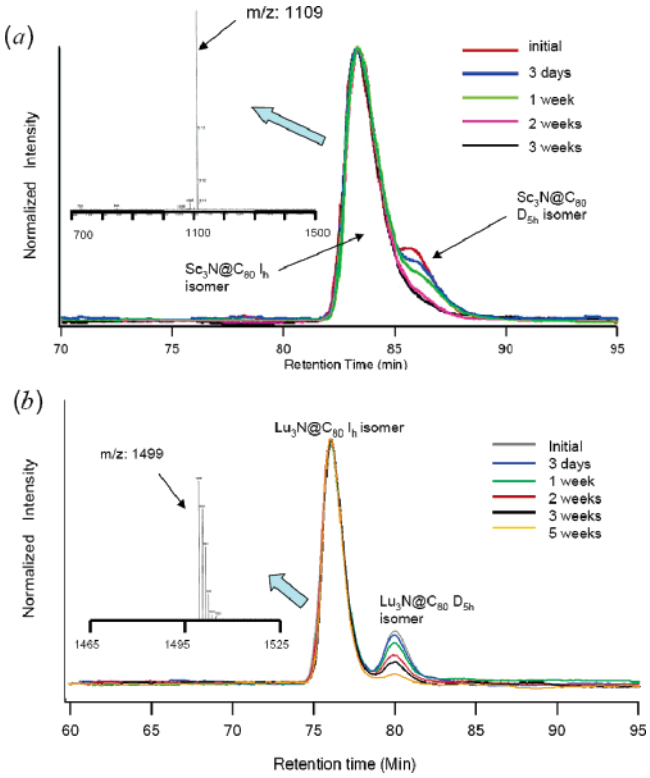

Figure 5. HPLC (PYE column, toluene, 1 mL/min, detection at 390 nm) traces. (a) The I_h and D_{5h} $Sc_3N@C_{80}$ mixture after reaction with resin **1** in toluene at room temperature for 0 day, 3 days, 1 week, 2 weeks, and 3 weeks. (b) The I_h and D_{5h} $Lu_3N@C_{80}$ mixture after reaction with resin **1** in toluene at room temperature for 0 day, 3 days, 1 week, 2 weeks, 3 weeks, and 5 weeks. The heights of the I_h $Sc_3N@C_{80}$ and $Lu_3N@C_{80}$ peaks were adjusted to be the same for all reaction times.

Scheme 1. Reaction of TNT-EMFs with Cyclopentadiene-Functionalized Resin **1**, A = Sc or Lu

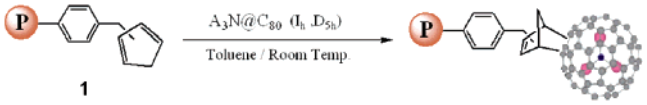

(18) Haddon, R. C.; Raghavachari, K. In *Buckminsterfullerenes*; Billups, W. E., Ciufolini, M. A., Eds.; VCH: New York, 1993; Chapter 7.
(19) Ge, Z.; Duchamps, J. C.; Cai, T.; Gibson, H. W.; Dorn, H. C. *J. Am. Chem. Soc.* **2005**, *127*, 16292−16298.
(20) (a) Aihara, J. *Phys. Chem., Chem. Phys.* **2001**, *3*, 1427−1431. (b) Aihara, J. *Chem. Phys. Lett.* **2001**, *343*, 465−469. (c) Aihara, J. *J. Phys. Chem. A* **2002**, *106*, 11371−11374.
(21) Campanera, J. M.; Bo, C.; Poblet, J. M. *Angew. Chem., Int. Ed.* **2005**, *44*, 7230−7233.
(22) Nakao, K.; Kurita, N.; Fujita, M. *Phys. Rev. B* **1994**, *49*, 11415−11420.

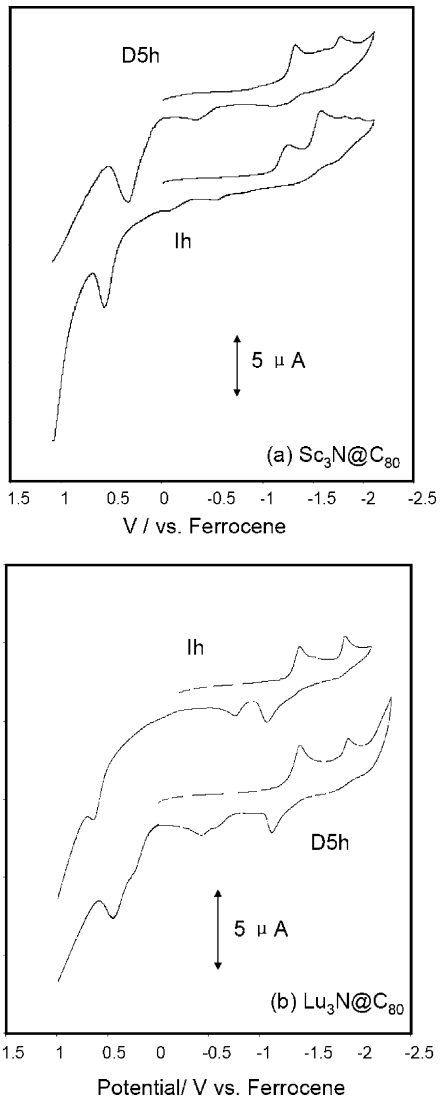

Figure 6. Cyclic voltammogram of the I_h and D_{5h} isomers of (a) $Sc_3N@C_{80}$ and (b) $Lu_3N@C_{80}$ in *o*-dichlorobenzene, 0.1 M $TBABF_4$, 500 mV/s scan rate.

different reactivities for I_h and D_{5h} TNT-EMFs toward resin **1** and the thermal reversibility of Diels−Alder cycloaddition,[19,23] it is feasible to establish a nonchromatographic strategy to separate both I_h and D_{5h} isomers; the resin produced after the D_{5h} isomer is consumed can be subjected to retro-Diels−Alder conditions to free this isomer (see Supporting Information for preliminary results). However, the purified D_{5h} samples utilized in the current study *vide infra* were purified by repetitive chromatographic methods.

b. Electrochemistry. The electrochemical behaviors of the I_h and D_{5h} isomers of $Sc_3N@C_{80}$ and $Lu_3N@C_{80}$ were determined by cyclic voltammetry (Figure 6), and the results are summarized in Table 1. Two reduction peaks and one oxidation peak were observed for each sample. The first reduction potentials ($^{red}E_1$) for the D_{5h} isomers of $Sc_3N@C_{80}$ (−1.333 V) and $Lu_3N@C_{80}$ (−1.409 V) are slightly more negative than those of the I_h isomers of $Sc_3N@C_{80}$ (−1.274 V) and $Lu_3N@C_{80}$ (−1.402 V), respectively. The oxidation potentials ($^{ox}E_1$) of both $Sc_3N@C_{80}$ and $Lu_3N@C_{80}$ D_{5h} isomers, however, are approximately 0.2 V less positive than those of the I_h isomers. The resulting electrochemical gaps ($^{ox}E_1-^{red}E_1$) for the D_{5h} isomers of $Sc_3N@C_{80}$ (1.675 V) and $Lu_3N@C_{80}$ (1.855 V) are approximately 0.18 V smaller than the electrochemical gaps for the I_h isomers of $Sc_3N@C_{80}$ (1.842 V) and $Lu_3N@C_{80}$ (2.044 V). The observation of less positive first oxidation potentials for the D_{5h} isomers is consistent with the assignments made by Echegoyen and co-workers from the cyclic voltammogram of the isomeric mixture of $Sc_3N@C_{80}$.[11]

It is worth noting that both oxidation and reduction potentials for I_h and D_{5h} isomers were shifted by changing the internal trimetallic nitride cluster. The electrochemical gap for $Lu_3N@C_{80}$ I_h (2.044 V) and D_{5h} isomers (1.855 V) are approximately 0.2 V larger than $Sc_3N@C_{80}$ I_h (1.842 V) and D_{5h} (1.675 V) isomers, respectively. However, the differences in the electrochemical gaps between the lanthanide TNT-EMFs are relatively small. For example, the electrochemical gap of I_h $Lu_3N@C_{80}$ (2.044 V) is comparable to that of I_h $Tm_3N@C_{80}$ (1.99 V).[24]

c. Theoretical Calculations. DFT calculations have provided the molecular orbital energy level diagrams of the isomers of $Sc_3N@C_{80}$ and $Lu_3N@C_{80}$ (Figure 7). The LUMOs of the D_{5h} isomers ($Sc_3N@C_{80} = -3.01$ eV, $Lu_3N@C_{80} = -2.94$ eV) are comparable to those of the I_h isomers ($Sc_3N@C_{80} = -2.91$ eV, $Lu_3N@C_{80} = -2.89$ eV). However, the HOMOs of the D_{5h} isomers ($Sc_3N@C_{80} = -5.29$ eV, $Lu_3N@C_{80} = -5.24$ eV) are higher than those of the I_h isomers ($Sc_3N@C_{80} = -5.45$ eV, $Lu_3N@C_{80} = -5.44$ eV). Therefore, the HOMO−LUMO gaps for the D_{5h} isomers are about 0.25 eV smaller than those of the I_h isomers. These are still relatively small differences and are perhaps in fortuitous agreement with the electrochemically determined potential differences (Table 1). They also agree well with the observation of the higher reactivity for D_{5h} isomers in the competition reactions with I_h isomers toward the cyclopentadiene-functionalized resin by Diels−Alder cycloaddition (Figure 5).

Interestingly, the I_h isomer of $La_2@C_{80}$ has almost the same HOMO level but a significantly different LUMO level compared with the I_h isomer of $Sc_3N@C_{80}$.[25] In contrast, for the same TNT cluster but different C_{80} cage symmetry, I_h vs D_{5h}, the changes of the HOMO levels are more obvious than those of the LUMO levels. Therefore, in general the LUMO energies of EMFs are more sensitive to the internal metallic cluster, while the HOMO levels are more sensitive to the structure and symmetry of the outside carbon cage, as expected on the basis of the $(A_3N)^{6+}C_{80}^{6-}$ formulation.[4b] Figure 7 shows that the HOMO levels of the I_h isomers are very different from those

Table 1. Electrochemical Redox Potentials (V versus Fc/Fc^+ in *o*-Dichlorobenzene, 0.1 M $TBABF_4$) and HOMO/LUMO Levels (eV) for the I_h and D_{5h} Isomers of $Sc_3N@C_{80}$ and $Lu_3N@C_{80}$

compound	$^{ox}E_1$	$^{red}E_1$	$^{ox}E_1-^{red}E_1$	HOMO	LUMO	HOMO–LUMO
$Sc_3N@C_{80}$ (I_h)	0.568	−1.274	1.842	−5.44	−2.91	2.53
$Sc_3N@C_{80}$ (D_{5h})	0.342	−1.333	1.675	−5.29	−3.01	2.28
$Lu_3N@C_{80}$ (I_h)	0.642	−1.402	2.044	−5.44	−2.89	2.55
$Lu_3N@C_{80}$ (D_{5h})	0.446	−1.409	1.855	−5.23	−2.94	2.29

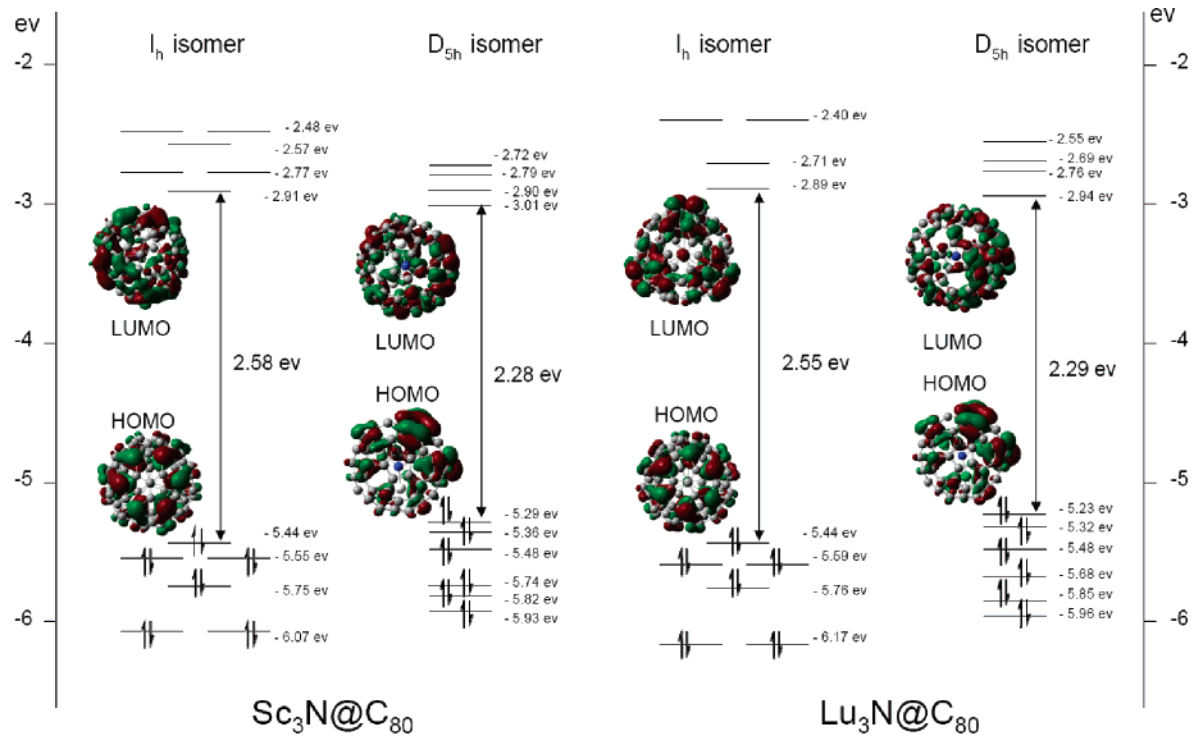

Figure 7. Molecular orbital (MO) diagrams of $Sc_3N@C_{80}$ and $Lu_3N@C_{80}$ (I_h and D_{5h} isomers).

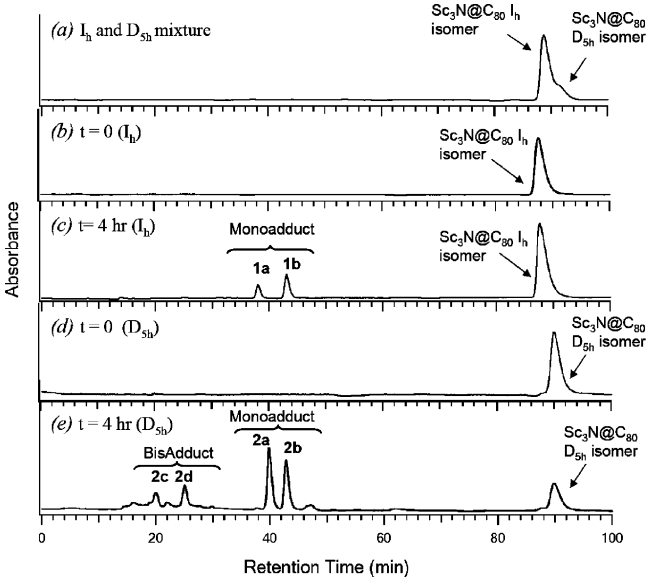

Figure 8. HPLC chromatograms: (a) mixture of $Sc_3N@C_{80}$ I_h and D_{5h} isomers, (b) pure $Sc_3N@C_{80}$ I_h isomer, (c) reaction mixture of the $Sc_3N@C_{80}$ I_h isomer with *N*-triphenylmethyl-5-oxazolidinone at ~132 °C for 4 h, (d) pure $Sc_3N@C_{80}$ D_{5h} isomer, and (e) reaction mixture of the $Sc_3N@C_{80}$ D_{5h} isomer with *N*-triphenylmethyl-5-oxazolidinone at ~132 °C for 4 h. HPLC conditions: 10 mm × 250 mm PYE at 1.0 mL min^{-1} flow rate with toluene, 390 nm detection. (Traces (b) and (c) are reproduced from ref 26.)

of the D_{5h} isomers, which are locally distributed onto one hemisphere. Similar to the localized LUMO for $La_2@C_{80}$ that results in high reactivity,[25] the higher reactivity of the D_{5h} isomer relative to the I_h isomer is presumably due to its more localized HOMO orbital.

In addition, the energy levels of HOMO and HOMO minus orbitals for $Sc_3N@C_{80}$ and $Lu_3N@C_{80}$ are similar, and the electron density distributions around both endohedral metallo-

Scheme 2. 1,3-Dipolar Cycloadditon Reaction of the D_{5h} isomer of $Sc_3N@C_{80}$ with *N*-Triphenylmethyl-5-oxazolidinone

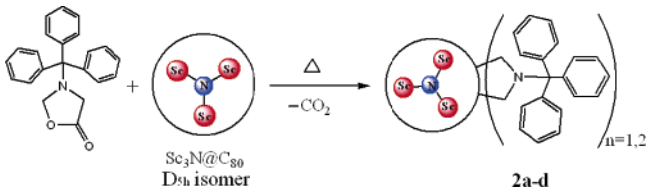

fullerenes are similar; this results from the six electrons transferred from the encapsulated cluster to the cage.

III. 1,3-Dipolar Cycloaddition Reaction of *N*-Tritylazomethine Ylide with D_{5h} $Sc_3N@C_{80}$. Recently, we reported the synthesis and characterization of mono- and di-(*N*-tritylpyrrolidino) derivatives of the I_h isomer of $Sc_3N@C_{80}$.[26] It was found that the addition of the *N*-tritylazomethine ylide occurs at both the 5,6- and 6,6-ring junctions of the $Sc_3N@C_{80}$ I_h cage, yielding the thermodynamic and kinetic products, respectively. In the present work, however, we have found that the D_{5h} isomer of $Sc_3N@C_{80}$ exhibits significantly higher reactivity with the 1,3-dipolar tritylazomethine ylide (Scheme 2) in comparison with the I_h isomer. The HPLC chromatogram of the original sample of $Sc_3N@C_{80}$ (Figure 8a) consisted mainly of the I_h isomer with a small amount of D_{5h} isomer, which appears as a shoulder at 91.0 min under slow flow rate conditions utilizing a PYE column. The purified $Sc_3N@C_{80}$ D_{5h} isomer (Figure 8d) was allowed to react with *N*-triphenylmethyl-5-oxazolidinone under

(23) (a) Guhr, K. I.; Greaves, M. D.; Rotello, V. M. *J. Am. Chem. Soc.* **1994**, *116*, 5997−5598. (b) Nie, B.; Rotello, V. M. *J. Org. Chem.* **1996**, *61*, 1870−1871.
(24) Krause, M.; Liu, X. J.; Wong, J.; Pichler, T.; Knupfer, M.; Dunsch, L. *J. Phys. Chem. A* **2005**, *109*, 7088−7093.
(25) Iiduka, Y.; Ikenaga, O.; Sakkuraba, A.; Wakahara, T.; Tsuchiya, T.; Maeda, Y.; Nakahodo, T.; Akasaka, T.; Kako, M.; Mizorogi, N.; Nagase, S. *J. Am. Chem. Soc.* **2005**, *127*, 9956−9957.
(26) Cai, T.; Slebodnick, C.; Xu, L.; Harich, K.; Glass, T. E.; Chancellor, C.; Fettinger, J. C.; Olmstead, M. M.; Balch, A. L.; Gibson, H. W.; Dorn, H. C. *J. Am. Chem. Soc.* **2006**, *128*, 6486−6492.

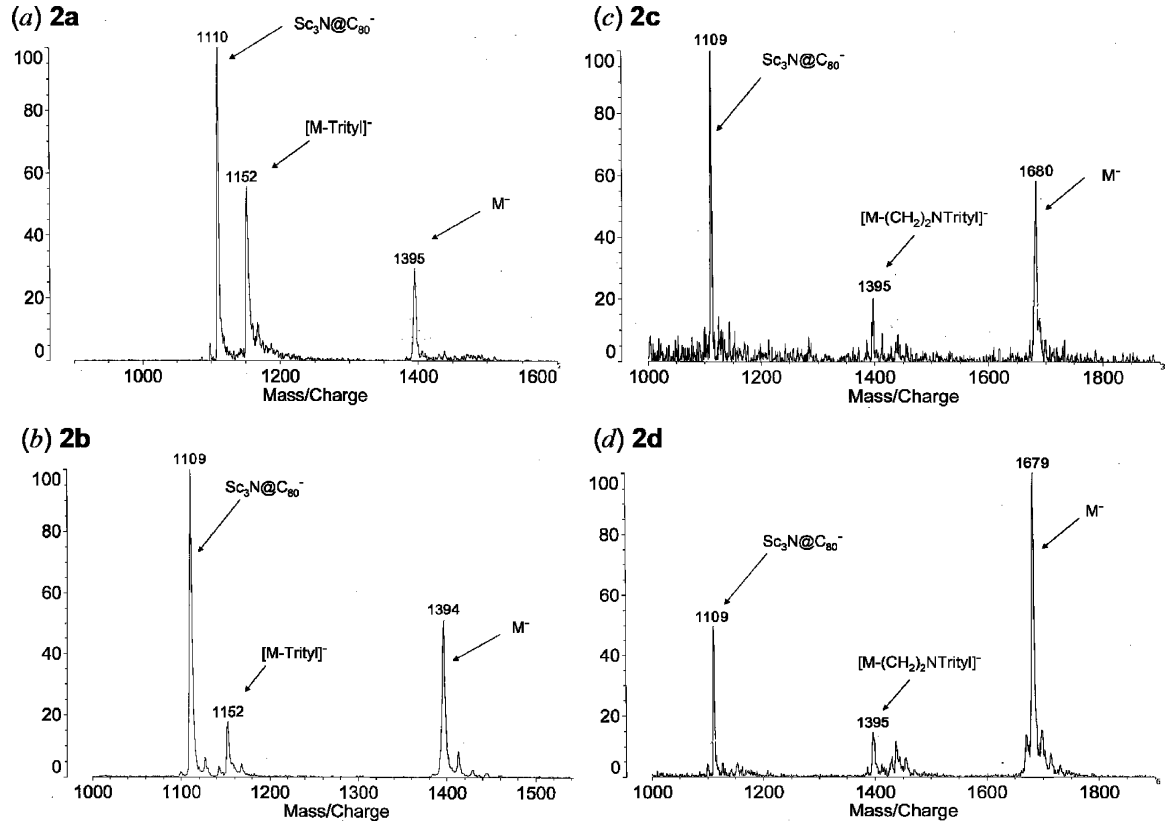

Figure 9. MALDI-TOF mass spectra using a 9-nitroanthracene matrix and negative ionization: (a) monoadduct **2a**, (b) monoadduct **2b**, (c) bisadduct **2c**, (d) bisadduct **2d**. Calculated for monoadducts: *m*/*z* 1394; calculated for bisadducts: *m*/*z* 1679.

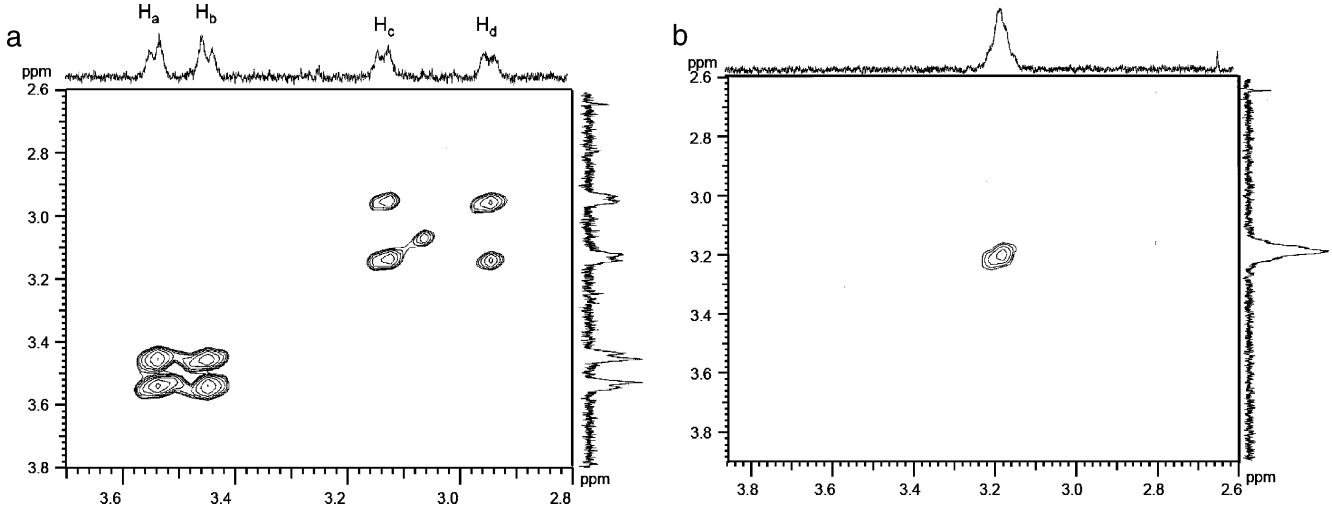

Figure 10. 500 MHz COSY spectra of the $Sc_3N@C_{80}$ D_{5h} isomer monoadducts **2a** (a) and **2b** (b) ([Solvent: 1,2-dichlorobenzene-d_4], 55 °C).

the same conditions as the I_h isomer.[26] After 4 h two strong peaks for monoadducts **2a** (40.0 min) and **2b** (43.0 min) were observed (Figure 8e) in contrast with the much weaker peaks observed for the I_h isomer (Figure 8c). In addition, the I_h isomer exhibited only one small peak for a bisadduct after 12 h of reaction time,[26] whereas two peaks were identified as the bisadducts (**2c**, **2d**) of the D_{5h} isomer after just 4 h of reaction time (Figure 8e). These data clearly indicate that the $Sc_3N@C_{80}$ D_{5h} isomer is more reactive than the I_h isomer. The mono- and bis-tritylpyrrolidino D_{5h} derivatives were characterized by MALDI-TOF mass spectra (Figure 9) and exhibited mass distribution patterns similar to those reported for the corresponding I_h derivatives.[26]

The ^{1}H NMR spectrum of **2a** exhibits four doublets (H_a, H_b, H_c, and H_d) for the methylene protons of the pyrrolidine ring. Moreover, the ^{1}H COSY spectrum of **2a** (Figure 10a) demonstrates that H_a-H_b and H_c-H_d are coupled with each other; this implies that H_a-H_b and H_c-H_d are on the two different methylene carbons, respectively. Unlike the spectrum of **2a**, in which the four methylene protons are in different chemical environments, the COSY spectrum of **2b** exhibits a broad singlet at 3.19 ppm (Figure 10b, Table 2), which indicates four equivalent methylene protons of the pyrrolidine ring.

There are a total of nine different types of C−C bonds on the D_{5h} C_{80} cage as shown in Figure 2; the statistical numbers of bonds of each type, ring junction, addition patterns, and bond

Table 2. NMR Chemical Shifts of Methylene Protons for $Sc_3N@C_{80}$ I_h Isomer Derivatives **1a** and **1b**;[a] D_{5h} Isomer Derivatives **2a** and **2b**

N-trityIpyrrolidino $Sc_3N@C_{80}$ derivative	δH (ppm)	rings junction	addition pattern[a]
I_h **1a**[b]	2.53(d), 3.95(d)	5,6	symmetric
I_h **1b**[b]	2.82(s), 3.11(s)	6,6	asymmetic
D_{5h} **2a**	3.53(d), 3.44(d), 3.13(d), 2.95(d)	6,6	asymmetic
D_{5h} **2b**	3.19 (s)	6,6	symmetric

[a] Addition pattern symmetry is based on the methylene carbons of the pyrrolidine ring on the derivatives. [b] Reference 26.

Table 3. D_{5h} $Sc_3N@C_{80}$: Comparison of X-ray and Computational Structural Parameters (Average Bond Lengths)

bond	bond numbers	rings junction	addition pattern[a]	expmtl bond length (Å)	theor calcd bond length (Å)	*N*-trityIpyrrolidino $Sc_3N@C_{80}$ D_{5h} derivative
a−a	10	5,6	symmetric	1.434	1.438	
a−b	10	6,6	asymmetric	1.420	1.427	**2a**[b]
b−c	20	6,6	asymmetric	1.419	1.430	**2a**[b]
c−c	10	5,6	symmetric	1.438	1.436	
c−d	20	5,6	asymmetric	1.451	1.451	
d−e	20	5,6	asymmetric	1.434	1.438	
d−f	20	6,6	asymmetric	1.432	1.437	**2a**[b]
e−e	5	6,6	symmetric	1.396	1.413	**2b**
f−f	5	6,6	symmetric	1.462	1.472	

[a] Symmetry is discussed based on the methylene carbons of the pyrrolidine ring on the derivatives. [b] Possible reaction sites for isomeric monoadduct **2a**.

lengths are summarized in Table 3. It is clear, from previous studies with the I_h pyrrolidino derivatives,[15,26,27] that the symmetric 5,6-ring junction adduct exhibits large chemical shift differences (1.2−1.4 ppm) for the diastereotopic methylene protons of the pyrrolidine ring, which are due to differential shielding effects from carbon cage ring currents and the nitrogen atom of the pyrrolidine ring. Since the ^{1}H NMR spectrum of **2b** exhibits only one singlet peak for the methylene protons of the pyrrolidine ring, the asymmetric 5,6-ring (c−d, d−e), the asymmetric 6,6-ring (a−b, b−c, d−f), and the symmetric 5,6-ring (a−a, c−e) junction adducts can be excluded as possible sites for cycloaddition adduct **2b**. As illustrated in Figure 2, only the e−e and f−f bonds can produce the symmetric 6,6-ring junction adduct **2b**. Furthermore, both experimental and theoretical calculated bond lengths demonstrate that e−e is the shortest bond and should be more reactive compared with the other bonds. Therefore, the pyracylene type e−e bond is the most likely addition site for the **2b** monoadduct (Table 3) as predicted from the crystallographic results. Based on the above discussions, and the limited ^{1}H COSY spectrum for **2a**, we predict that **2a** is the asymmetric 6,6-ring junction cycloaddition adduct. The three most likely cycloaddition sites for adduct **2a** are at the a−b, b−c, and d−f bonds as summarized in Table 3, and further studies to elucidate this structure are in progress.

In a previous study we found that upon heating the 6,6-ring junction adduct of the I_h isomer converted into the 5,6-ring junction adduct, and we proposed a single bond migration mechanism based on the concept of microscopic reversibility.[26] After 3 h in a solution of 1,2-chlorobenzene-d_4 at 160 °C purified isomer **2b** was unchanged, whereas, under these conditions, **2a** was partially converted to other unidentified monoadduct isomers. As expected, these results also indicate that **2b** is the thermodynamically stable product. There is remarkable similarity in the cycloaddition reactions of the D_{5h} and I_h isomers of $Sc_3N@C_{80}$ in providing only two monoadducts. However, a key difference is the presence of the pyracylene motif in the D_{5h} isomer, which undoubtedly leads to the enhanced reactivity of the D_{5h} $Sc_3N@C_{80}$ isomer. This is consistent with reactivity patterns for empty-cage fullerenes. We are currently investigating the regioselectivity of D_{5h} C_{80} cages with other metal clusters (e.g., yttrium, holmium, thulium, etc.).

Conclusions

The structure of the D_{5h} isomer of $Sc_3N@C_{80}$ has been determined crystallographically. The planar Sc_3N portion is tipped out of the noncrystallographic, horizontal mirror plane of the carbon cage by 30°. The short C−C bond length and high degree of pyramidization for the central carbon atoms of the pyracylene sites of the D_{5h} isomer of $Sc_3N@C_{80}$ suggest that these C−C bonds are the ones most likely to undergo addition reactions.

The D_{5h} isomers of $Sc_3N@C_{80}$ and $Lu_3N@C_{80}$ exhibit higher reactivity than the I_h isomers toward cyclopentadiene-functionalized resin **1** under Diels−Alder cycloaddition. Both cyclic voltammetry and theoretical molecular orbital (MO) calculations demonstrate that the D_{5h} isomers have smaller energy gaps than those of the I_h isomers, which is consistent with the observation of higher reactivity for the D_{5h} isomers. The differences between the first oxidation potentials and HOMO levels for the I_h and D_{5h} isomers are larger than those of the reduction potentials and LUMO levels; these results show that, as expected on the basis of the transfer of six electrons from the cluster to the C_{80} carbon cage, the isomeric nature of the cage structure plays a more important role in determining the HOMO level than the internal metallic cluster.

The D_{5h} $Sc_3N@C_{80}$ isomer also proves to be more reactive toward 1,3-dipolar cycloaddition of *N*-tritylazomethine ylide than the I_h isomer under same reaction conditions. Two D_{5h} $Sc_3N@C_{80}$ monoadducts and two bisadducts were isolated and characterized by MALDI-TOF MS spectroscopies. Monoadduct **2a** is assigned as an asymmetric product based on its ^{1}H NMR and COSY spectra. Monoadduct **2b** exhibits a single methylene proton signal in its ^{1}H NMR spectrum, which indicates a symmetrical addition at the 6,6-ring junction in the pyracylene unit, consistent with its highly reactive character. Preliminary studies show that monoadduct **2b** is thermally stable to isomerization, but **2a** is converted to other products upon heating.

Experimental Section

Materials and Methods. The $Sc_3N@C_{80}$ and $Lu_3N@C_{80}$ I_h and D_{5h} isomer mixture was obtained by the chemical separation method.[19] Pure $Sc_3N@C_{80}$ I_h and D_{5h} isomers were isolated from the mixture by HPLC using a PYE column, with toluene @ 1.0 mL/min, $\lambda = 390$ nm. Toluene (HPLC Grade ≥ 99.9%) and *o*-dichlorobenzene (99.9%) were used as

(27) Yamada, M.; Wakahara, T.; Nakahodo, T.; Tsuchiya, T.; Maeda, Y.; Akasaka, T.; Yoza, K.; Horn, E.; Mizorogi, N.; Nagase, S. *J. Am. Chem. Soc.* **2006**, *128*, 1402−1403.

obtained from Aldrich. A semipreparative PYE [β2-(1-pyrenyl)ethyl silica] column (10 mm × 250 mm) and a guard PYE column (10 mm × 20 mm) were used for both analysis and purification. HPLC system: Acure series III pump, 757 Absorbance Detector (Applied Biosystems).

The ^{13}C NMR spectrum of the $Lu_3N@C_{80}$ D_{5h} isomer was obtained by using a Varian Inova 800 instrument (Georgia Institute of Technology). The $Lu_3N@C_{80}$ D_{5h} isomer sample was dissolved in CS_2/D−acetone (v/v: 10/1) and doped with chromium acetylacetonate. A JEOL ECP 500 MHz instrument was used for the $Sc_3N@C_{80}$ D_{5h} derivatives' ^{1}H NMR and COSY measurements.

Cyclic voltammetric measurements were conducted using a CH Instruments model 600A potentiostat (Austin, TX) and a microelectrochemical cell described previously.[28] This cell allows measurement down to 50 μL of sample solution. Measurements were conducted using 1,2-dichlorobenzene solutions containing 0.100 M tetra-*n*-butylammonium tetrafluoroborate and an approximately 5×10^{-4} M concentration of the TNT fullerene. Potentials are reported relative to the reversible ferrocene oxidation couple. Solution resistance was compensated 95% for all measurements.

X-ray Crystallography and Data Collection. The crystals were removed from the glass tube in which they were grown together with a small amount of mother liquor and immediately coated with a hydrocarbon oil on the microscope slide. A suitable crystal was mounted on a glass fiber with silicone grease and placed on the goniometer head in the cold dinitrogen stream from a CRYO Industries low-temperature apparatus at 90(2) K. The diffractometer was a Bruker SMART Apex with an Apex II CCD and utilized Mo Kα radiation. No decay was observed in 50 duplicate frames at the end of data collection. Crystal data are given below. The structure was solved by direct methods and refined using all data (based on F^2) with the software of SHELXTL 5.1. A semiempirical method utilizing equivalents was employed to correct for absorption.[29] Hydrogen atoms were added geometrically and refined with a riding model.

Crystal Data for $C_{128}H_{56}N_5NiSc_3$. Black parallelepiped, triclinic, space group $P\bar{1}$, $a = 14.505(3)$ Å, $b = 14.878(3)$ Å, $c = 19.855(4)$ Å, $\alpha = 85.052(3)°$, $\beta = 86.758(3)°$, $\gamma = 61.016(3)°$, $V = 3733.6(12)$ Å^3, $Z = 2$, $D_c = 1.652$ Mg/m^3, $T = 90(2)$ K; R1 = 0.112, wR2 = 0.124 for all data; conventional R1 = 0.052 computed for 13 289 observed data ($I > 2\sigma(I)$) with 0 restraints and 1235 parameters.

Computations. Full geometry optimizations were conducted at the B3LYP level[30−32] using the Gaussian 03 program.[33] The effective core potential and the corresponding basis set were used for Sc and Lu. The basis sets employed were LanL2DZ for Sc,[34] *Stuttgart RSC Segmented/ECP* for Lu,[35] and 6-31G* for C and N.[36] For the computed structure of $Sc_3N@C_{80}$, we referred to the crystallographic data. We have assumed that $Lu_3N@C_{80}$ exhibits a structure similar to that of $Sc_3N@C_{80}$ for the computations. All the calculations (I_h and D_{5h}) are subject to frequency analyses, which are performed at the same level as that of the geometry optimization. As a result, no imaginary frequencies are reported for optimized structures.

Synthesis of *N*-Tritylpyrrolidino Derivatives of the D_{5h} Isomer of $Sc_3N@C_{80}$. A solution of 0.4 mg (0.4 μmol) of $Sc_3N@C_{80}$ D_{5h} isomer and 6 mg (0.02 mmol) of *N*-triphenylmethyl-5-oxazolidinone in 7 mL of chlorobenzene was heated at reflux under nitrogen. The solvent was removed by a rotary evaporator. The crude solid was dissolved in toluene and then injected into an HPLC for analysis. **2a**, **2b**, **2c**, and **2d** were isolated by HPLC using a PYE column, with toluene @ 1.0 mL/min, $\lambda = 390$ nm.

Acknowledgment. We are grateful for support of this work by the National Science Foundation [(CHE-0413857 (A.L.B.), CHE-0443850 (H.C.D.), DMR-0507083 (H.C.D., H.W.G.)] and the National Institute of Health [1R01-CA119371-01 (H.C.D., H.W.G.)].

Supporting Information Available: Complete list of authors for ref 33. X-ray crystallographic data for the D_{5h} isomer of $Sc_3N@C_{80}$·Ni(OEO)·2benzene in CIF format. Scheme for purification of $Sc_3N@C_{80}$ I_h and D_{5h} isomers. This material is available free of charge via the Internet at http://pubs.acs.org.

JA0615573

(28) Anderson, M. R.; Dorn, H. C.; Stevenson, S. A. *Carbon* **2000**, *38*, 1663−1670.
(29) SADABS 2.10, G. M. Sheldrick, based on a method of R. H. Blessing, *Acta Crystallogr., Sect. A* **1995**, *A51*, 33.
(30) Becke, A. D. *Phys. Rev. A* **1988,** *38*, 3098−3100.
(31) Becke, A. D. *J. Chem. Phys.* **1993**, *98*, 5648−5652.
(32) Lee, C.; Yang, W.; Parr, R. G. *Phys Rev. B* **1988**, *37*, 785−789.
(33) Frisch, M. J. et al. Gaussian, Inc., Pittsburgh, PA, 2003. Frisch, M. J. et al. *GAUSSIAN 03*, revision B.05; Gaussian Inc.: Wallingford, CT, 2004.
(34) Hay, P. J.; Wadt, W. R. *J. Chem. Phys.* **1985**, *82*, 284−298.
(35) Cao, X.; Dolg, M. *J. Chem. Phys.* **2001**, *115*, 7348. Cao, X.; Dolg, M. *THEOCHEM* **2002**, *581*, 139.
(36) Hehre, W. J.; Ditchfield, R.; Pople, J. A. *J. Chem. Phys.* **1972**, *56*, 2257−2261.